New Folder Name_____

Magnetic Feild Measurements

Magnetic Field Measurements

Martin W. Regehr

May 29, 1990

1 Introduction

There has been some concern that time-varying magnetic fields in the laboratory may eventually hurt the performance of the 40m interferometer by producing motions of suspended components equipped with magnets for position control. This report describes some recently made measurements of magnetic fields and estimates the apparent displacements produced in the proposed beamsplitter and in the test masses by these magnetic fields.

2 Mechanisms Coupling Magnetic Fields and Apparent Displacements

A spatially non-uniform magnetic field $\vec{B}$ will produce a force $\vec{F}$ on a magnet of magnetic moment $\vec{\mu}$ given approximately by

$$\begin{aligned} \vec{F} &= (\vec{\mu}\cdot\vec{\nabla})\vec{B} \\ &= \mu[\tfrac{\partial B_x}{\partial z}\vec{e}_x] \end{aligned} \tag{1}$$

for $\vec{\mu} = \mu\vec{e}_z$ and $\mu = |\vec{\mu}|$.

For a field with time dependence $e^{i\omega t}$, this force will produce a displacement of

$$\vec{X} = -\frac{n}{m\omega^2}\vec{F} \tag{2}$$

where m is the mass of the suspended component and n is the number of magnets on it. Substituting the following values for the beamsplitter and test mass:

		Beamsplitter	Test Mass
	m (kg)	0.12	1.6
	n	3	2
	μ (Am^2)	3.0×10^{-2}	0.14
yields:	$\frac{X}{\frac{\partial B_x}{\partial z}}[(\frac{1kHz}{f})^2$ m^{2}T$^{-1}]$	1.9×10^{-8}	4.4×10^{-9}

A spatially uniform magnetic field (with the same time dependence as above) will produce a torque $\vec{\tau} = \vec{\mu} \times \vec{B}$ which will cause the suspended component to rotate about its center of mass. If the offset between the beam and the center of mass is (arbitrarily) 1 cm, then the apparent displacement is $X = \alpha(0.01\text{m})$ where α is the angular displacement, $\alpha = \frac{n\tau}{\mathcal{I}\omega^2}$ and $\mathcal{I}$ is the moment of inertia of the suspended component. Then

	Beamsplitter	Test Mass
$\mathcal{I}$ (kg m^2)	8.9×10^{-5}	3.0×10^{-3}
n	3	2
μ (A m^2)	3.0×10^{-2}	0.14
$\frac{X}{B}[(\frac{1kHz}{f})^2$ m T$^{-1}]$	2.6×10^{-7}	2.4×10^{-8}

Angular displacement can also produce apparent displacement by causing the beam to couple into higher order cavity modes. For the beamsplitter this effect is approximately 7 orders of magnitude smaller than the effect described above; it has not yet been calculated for the test masses.

The spatially uniform magnetic field will generate eddy currents in any conductor immersed in it, and these will produce non-uniformities which produce forces on the magnets [1]. For the beamsplitter , one such conductor is the cage holding the OSEM's. The calculation deriving the field gradient $\frac{\partial B_z}{\partial z}$ produced this way is reproduced in Appendix A; its result is

$$\frac{\partial B_z}{\partial z} = (17\text{m}^{-1})B \tag{3}$$

The coils used to drive the magnets are another set of such conductors. If we model the coil as a filamentary perfect conductor in series with an impedance Z, the current in the coil (radius r, N turns) will be $I = N\omega\pi r^2 B/Z$, and

$$(\frac{\partial B_z}{\partial z})_{max} = (1.7\times10^{-6}\text{Hm}^{-1})(\frac{\omega}{Z})N^2B \tag{4}$$

For the OSEM and test mass coils, $|Z|$ is approximately 54Ω and 62Ω for frequencies less than 5 kHz and 10 kHz, respectively, so

	Beamsplitter	Test Mass
$\frac{\frac{\partial B_z}{\partial z}}{B}[(\text{m}^{-1})(\frac{f}{1\text{kHz}})]$	15	6.9
$\frac{X}{B}[\text{mT}^{-1}(\frac{1kHz}{f})]$	2.9×10^{-7}	3.0×10^{-8}

3 Apparatus

Two sensors were used to make the measurements. Sensor 1 consists of two coils of 500 turns each and 8.3 cm diameter, wound 8.2 cm apart on a lucite tube. The tube also holds four BNC connectors to allow access to both ends of each

coil, and is shielded with a copper foil shield, broken to prevent eddy currents from flowing around the circumference. This sensor is usually used with one end of one coil connected to one end of the other; the voltage at the two remaining terminals is then either the sum or the difference of the EMF's induced in the two coils. These two configurations will be referred to as sensor 1a and sensor 1b, respectively. Sensor 2 is a coil of 7483 turns and 9.2 cm diameter, with a single BNC connector and a partial brass foil shield. The sensors were used with an EG&G PARC 113 preamplifier and a HP 3562A spectrum analizer. A 65 turn, 65 cm diameter coil was used with the "LOUIS" coil driver, a waveform generator and an oscilloscope to calibrate the sensors.

4 Experimental Method

The response of sensors 1b and 2 was measured using circuits similar to that of Fig. 1a. For sensor 1b, this served to confirm that it behaves essentially as an ideal coil in the frequency range of interest, the first resonance being at 62kHz, and the response not deviating measurably from flatness below about 20 kHz. For sensor 2, a resonance was found at 2.1 kHz, where the ratio of the voltage measured with the switch open to that with the switch closed ranged from 50 to 70 (during several repetitions of the measurement). This measurement of the amplification on resonance was not useful for determining the sensitivity of the coil to magnetic fields since the large currents flowing at resonance affect the field, but it is the correct amplification factor to use when calculating the Johnson noise spectrum expected from the coil. Another calibration involved passing a known current through the calibration coil described above and measuring the voltage pickup in the sensors. Sensors 1a and 2 were calibrated at the center of the calibration coil, their axes aligned with its axis, and sensor 1b was calibrated in the same orientation, at that location on the axis of the calibration coil where it gave the maximum pickup (this point lay about one-half calibration-coil-radius above center, as expected). The voltage measured was, to within 25%, just the expected induced EMF, with two exceptionns: Sensor 1b picked up as much signal at the center of the calibration coil as would be expected from 160 turns of the same size as those in sensor 1, and sensor 2 showed amplification of the signal above about 1 kHz and peaking at 2.1 kHz with an amplification of about 9. An attempt to measure the electrostatic pickup in sensor 1b was made using the circuit of Fig 1b. This pickup was found to be smaller than 10 nV/rHz (the measured input voltage noise of the preamplifier) in the frequency range 0 - 2.5 kHz.

Magnetic field measurements were performed in various places at the Louie end of the 40m lab, with the fluorescent lights shut off. The preamplifier poles were set to 1 Hz and 10 kHz, its gain at 1000, and it was run on batteries.

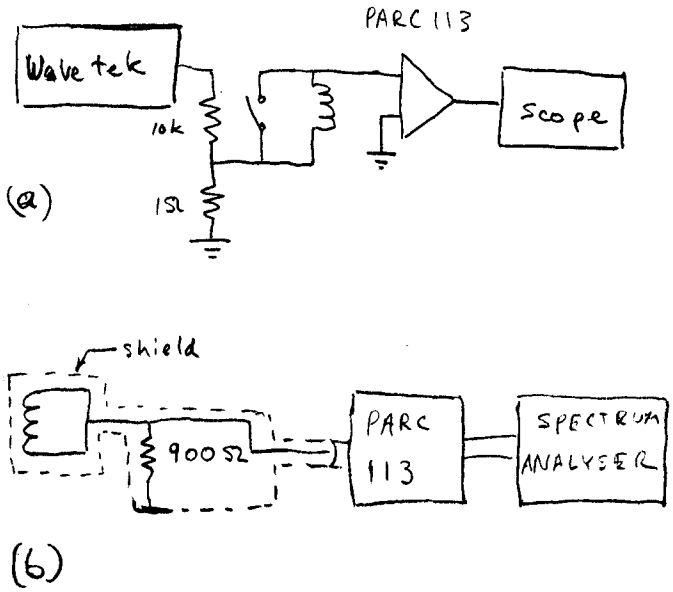

Figure 1: Voltage Response Test Circuit (a) and Electrostaic Pickup Test Circuit (b)

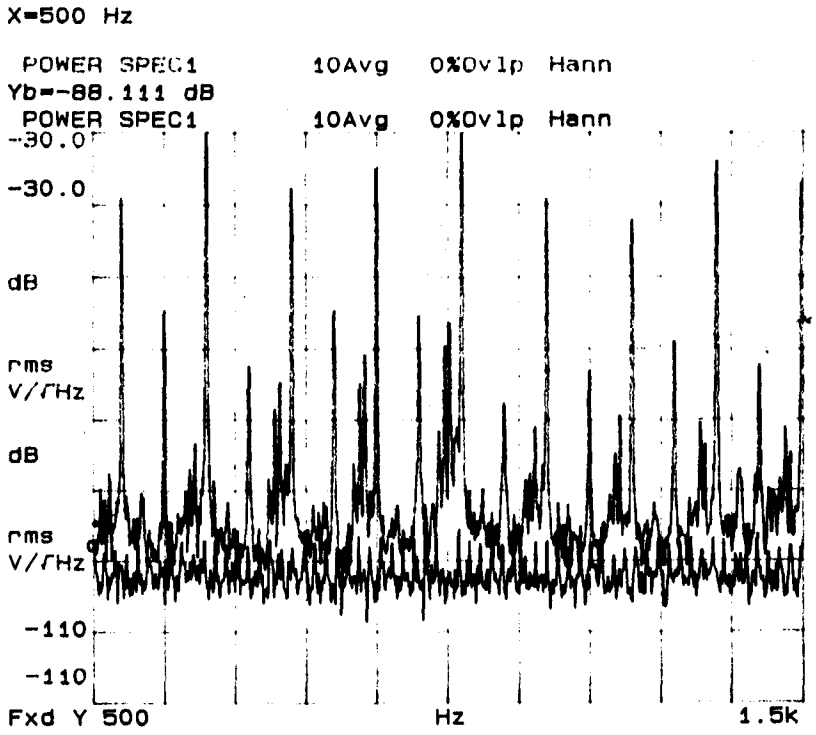

Figure 2: Sensor 2 Spectrum

5 Results

It was found that the spectra measured can generally be decomposed into a sum of four components. The following is a description each type of feature and a summary of the typical magnitude of the displacement of optical components it is estimated to produce.

1. **A minimum noise level, or floor, for which no part of any spectrum falls below it.** In this set of measurements, the floor always corresponds to preamplifier noise or spectrum analyser input noise or Johnson noise in the coil. For the magnetic field, this measurement limit corresponds to a spectral density of $1.8\times10^{-13}(\frac{1\text{kHz}}{f})$ T/$\sqrt{\text{Hz}}$ below about 1 kHz; near 2 kHz sensor 2 becomes limited by its Johnson noise and the limit at 2.1 kHz corresponds to 5.3×10^{-14}T/$\sqrt{\text{Hz}}$ (see Fig.'s 2 and 3). The displacements corresponding to this spectral density of magnetic field are smaller than those corresponding to the $\frac{\partial B_z}{\partial z}$ noise floor. For $\frac{\partial B_z}{\partial z}$ (see Fig. 4), this measurement limit corresponds to a spectral den-

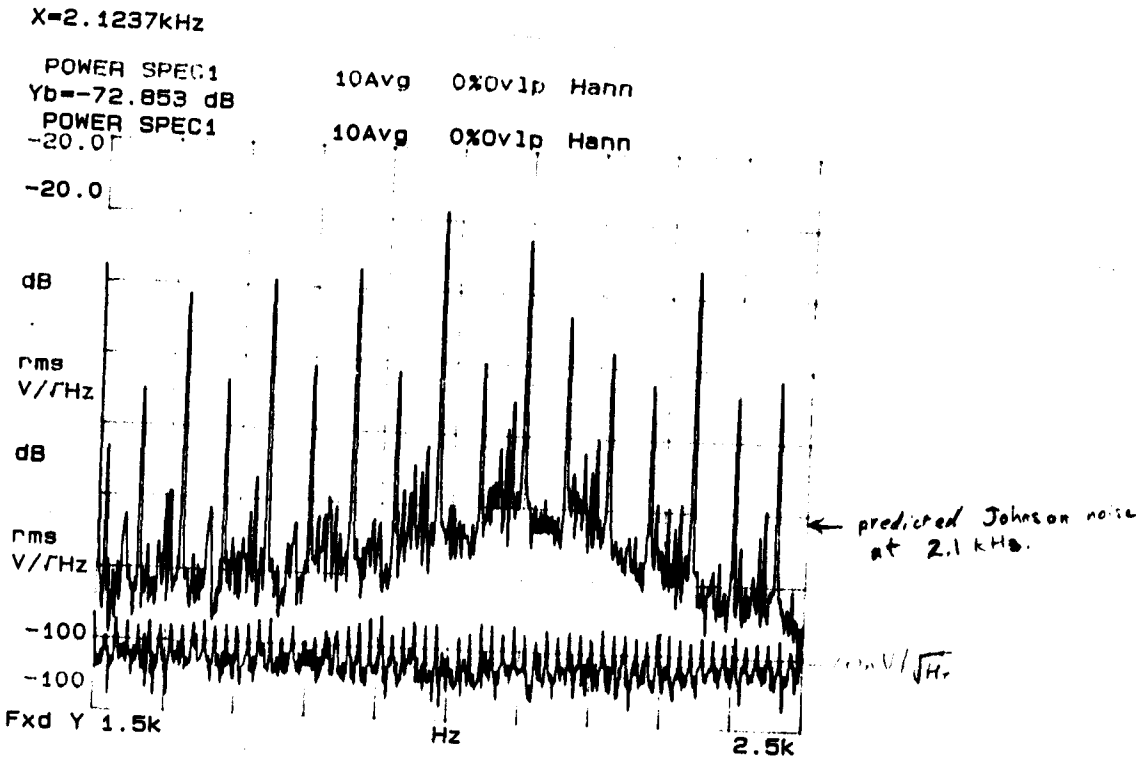

Figure 3: Sensor 2 Spectrum

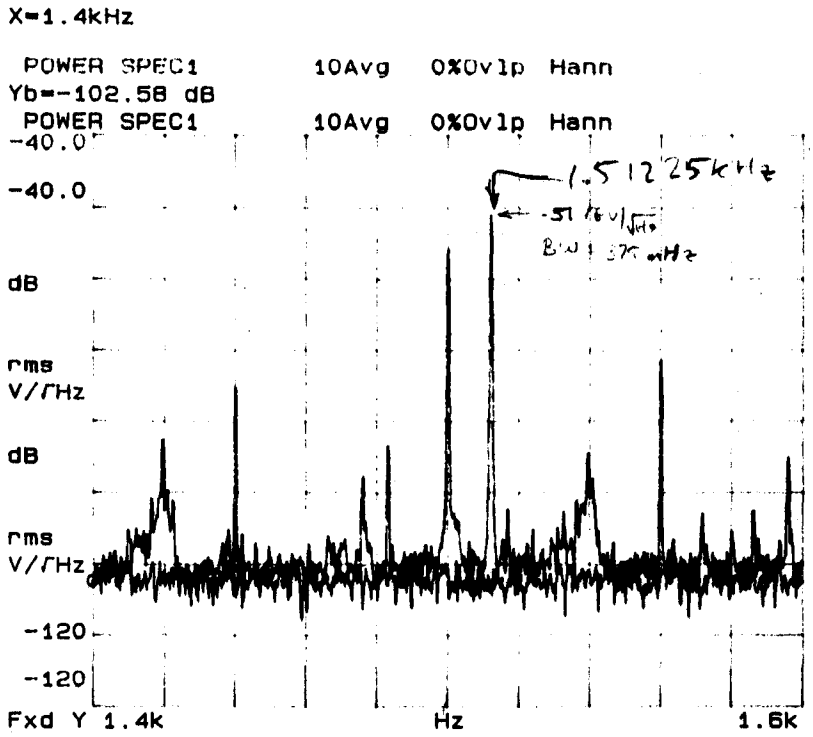

Figure 4: Sensor 1b Spectrum

sity of $7.1\times10^{-12}(\frac{1\text{kHz}}{f})$ T/m$\sqrt{\text{Hz}}$, which corresponds to a displacement spectral density of $1.3\times10^{-19}(\frac{1\text{kHz}}{f})^3$ m/$\sqrt{\text{Hz}}$ for the beamsplitter and $3.0\times10^{-20}(\frac{1\text{kHz}}{f})^3$ m/$\sqrt{\text{Hz}}$ for the test mass.

2. **Sharp, unresolved peaks at multiples of 60 Hz.** The magnetic field spectrum (see Fig. 5) has a peak of $1.3\times10^{-10}\text{T}_{rms}$ at 1020 Hz; the corresponding displacements are $4.2\times10^{-17}\text{m}_{rms}$ in the beamsplitter and $3.9\times10^{-18}\text{m}_{rms}$ in the test mass. The $\frac{\partial B_z}{\partial z}$ spectrum (see Fig. 4) has a peak of $4.6\times10^{-10}(\text{Tm}^{-1})_{rms}$ at 1500 Hz; the corresponding displacements are $3.7\times10^{-18}\text{m}_{rms}$ in the beamsplitter and $8.9\times10^{-19}\text{m}_{rms}$ in the test mass.

3. **Sharp, unresolved peaks at frequencies which are not multiples of 60 Hz.** The magnetic field spectrum (see Fig. 6) has a peak of $1.1\times10^{-11}\text{T}_{rms}$ at 1003 Hz; the corresponding displacements are $3.6\times10^{-18}\text{m}_{rms}$ in the beamsplitter and $3.3\times10^{-19}\text{m}_{rms}$ in the test mass. The $\frac{\partial B_z}{\partial z}$ spectrum (see Fig. 4) has a peak of $8.3\times10^{-10}(\text{Tm}^{-1})_{rms}$ at 1512 Hz; the

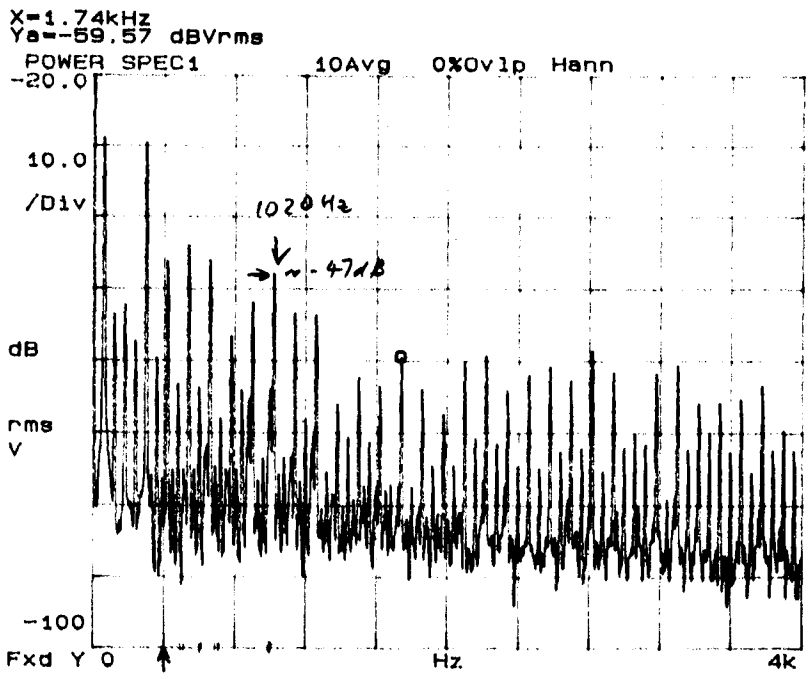

Figure 5: Sensor 1a Spectrum

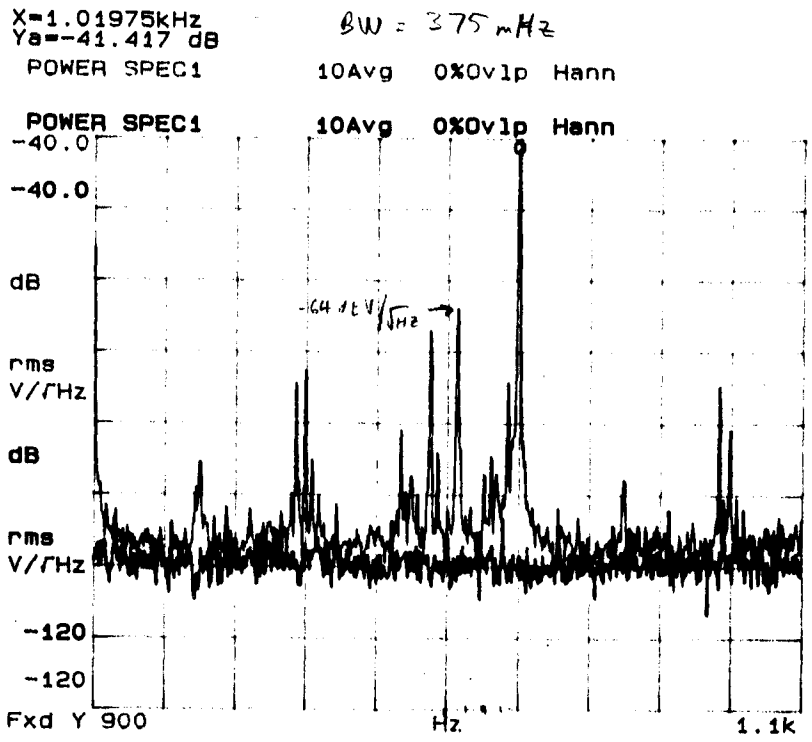

Figure 6: Sensor 1a Spectrum

corresponding displacements are $7.0\times10^{-18}\mathrm{m}_{rms}$ in the beamsplitter and $1.6\times10^{-18}\mathrm{m}_{rms}$ in the test mass.

4. **Broader, resolved peaks, of width about 10 to 20 Hz, usually accompanied by other peaks of similar shape at 60 Hz intervals.** The magnetic field spectrum (see Fig. 6) has a peak of $9.9\times10^{-13}\mathrm{T}/\sqrt{\mathrm{Hz}}$ at 930 Hz; the corresponding displacements are $3.2\times10^{-19}\mathrm{m}/\sqrt{\mathrm{Hz}}$ in the beamsplitter and $3.5\times10^{-20}\mathrm{m}/\sqrt{\mathrm{Hz}}$ in the test mass. The $\frac{\partial B_z}{\partial z}$ spectrum (see Fig. 4) has peaks of $1.5\times10^{-11}\mathrm{Tm}^{-1}/\sqrt{\mathrm{Hz}}$ at 1420 and 1540 Hz; the corresponding displacements are $1.5\times10^{-19}\mathrm{m}/\sqrt{\mathrm{Hz}}$ in the beamsplitter and $2.9\times10^{-20}\mathrm{m}/\sqrt{\mathrm{Hz}}_{rms}$ in the test mass.

6 Appendix A

To calculate the non-uniformities introduced in the field by the conducting OSEM cage, the cage was modelled as a set of conducting loops, as shown in Fig. 7. The conductivity of the loops was assumed infinite, so that the current in each loop (due to the induced EMF) is limited only by the self-inductance of the loop. Rather than evaluate this inductance exactly, a pessimistic estimate (one which will predict a larger than accurate non-uniformity in the field) was made: $\Phi = B_{center}A$, where Φ is the flux threading the loop (of area A and radius r), and B_{center} is the (eddy current induced) magnetic field at its center, $B_{center} = \mu_0 I/2r$. This gives a self-inductance of $L = \Phi/I = \mu_0\pi r/2$. Making these assumptions turns out to be equivalent to assuming an eddy current in each loop which just cancels the externally applied magnetic field at the center of that loop.

Using this assumed value for the current, the relevant derivatives of the magnetic field were calculated numerically from Hart's tables [2].

References

[1] Seiji Kawamura, private communication

[2] Hart P J 1967 *Universal Tables for Magnetic Fields of Filamentary and Distributed Circular Elements* (New York: Elsevier)

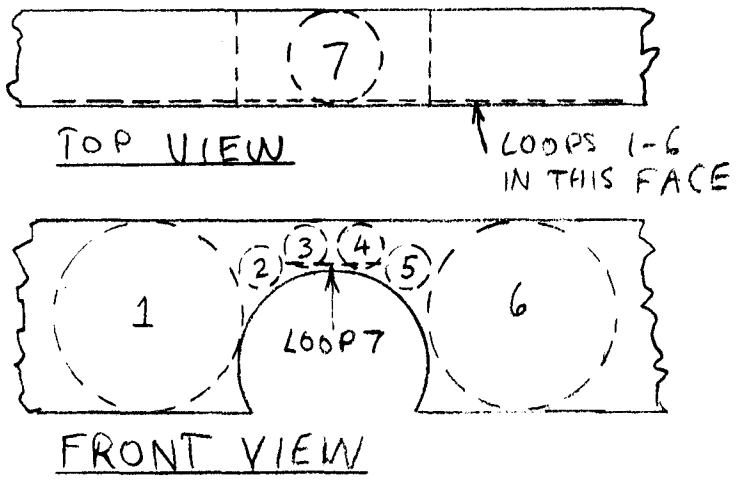

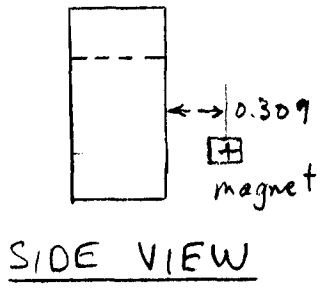

Figure 7: Location and Size of Loops Used to Model the Conductor (To Scale)